Available online at www.sciencedirect.com
ScienceDirect
Acta Biomaterialia 5 (2009) 63–75
Acta BIOMATERIALIA
www.elsevier.com/locate/actabiomat

Nanocomposite hydroxyapatite formation on a Ti–13Nb–13Zr alloy exposed in a MEM cell culture medium and the effect of H_2O_2 addition

M.A. Baker [a,*], S.L. Assis [b], O.Z. Higa [b], I. Costa [b]

[a] *The Surface Analysis Laboratory, Faculty of Engineering and Physical Sciences, University of Surrey, Guildford, Surrey GU2 7XH, UK*
[b] *IPEN/CNEN-SP, Av. Prof. Lineu Prestes 2242, CEP 05508-900, São Paulo, Brazil*

Received 19 March 2008; received in revised form 23 July 2008; accepted 12 August 2008
Available online 29 August 2008

Abstract

Titanium alloys are known to nucleate an apatite layer when in contact with simulated body fluid. This improves the bioactivity of titanium implants and accelerates osseointegration. Promoting the formation of hydroxyapatite on biocompatible metals is, therefore, a very important topic of biomaterials research. In this paper, the formation of hydroxyapatite (HA) on the near-β Ti–13Nb–13Zr alloy by immersion in minimal essential medium (MEM), with and without H_2O_2 addition, has been studied using electrochemicals methods, scanning electron microscopy and X-ray photoelectron spectroscopy. The in vitro biocompatibility of this alloy was evaluated by cytotoxicity tests. The Ti–13Nb–13Zr alloy exhibits passive behaviour over a wide potential range in MEM and the passive film is composed of an inner barrier layer and an outer porous layer. The addition of H_2O_2 leads to a thickening of the outer porous layer and strongly reduced current density. With regard to the surface composition, immersion in MEM solution results in the formation of an island-like distribution of HA + amino acids. Addition of H_2O_2 to the MEM solution strongly promotes the formation of a thicker, continuous but porous nanocomposite layer of HA + amino acids. The Ti–13Nb–13Zr alloy is non-toxic and the nanocomposite HA + amino acid layer formed in the MEM solution favours the growth of osteoblast cells. For Ti alloys, the release of H_2O_2 in the anti-inflammatory response appears to be an important beneficial process as it accelerates osseointegration.

Keywords: Ti–13Nb–13Zr; Hydroxyapatite; XPS; MEM; H_2O_2

1. Introduction

The excellent corrosion resistance of Ti alloys is due to a thin and adherent oxide film on their metallic surface. This film is spontaneously formed by exposure of the Ti alloy to the atmosphere or to aerated environments owing to the high affinity of Ti for oxygen. Due to this fact, when the oxide film is damaged it can be easily repaired even when oxygen is present at low partial pressures (ppm). Although the oxide film on Ti and Ti alloys is highly stable, when these materials are used as implants, electrochemical reactions with physiological fluids can occur which are intensified by the combined interaction of corrosion and mechanical stresses and/or wear. Two general reviews on the surface modification and studies of surface interactions of Ti and Ti alloys in biomedical applications have been given by Jones [1] and Liu et al. [2].

The electrochemical reactions occurring at the surface of Ti implants are affected by the surface characteristics such as composition, structure, roughness, morphology and composition of the physiological body fluids [3]. The composition, thickness and nature of the oxide film on Ti alloys depend on the environment to which it is exposed. McCafferty and Wightman [4] have undertaken X-ray photoelectron spectroscopy (XPS) of the native oxide on pure Ti and shown it to be comprised solely of TiO_2, together with a strong outer hydroxide component and adsorbed water. However, importantly, they quoted the oxide thickness to be approximately 8 nm and accordingly did not

* Corresponding author. Tel.: +44 1483 686294; fax: +44 1483 686291.
E-mail address: m.baker@surrey.ac.uk (M.A. Baker).

1742-7061/$ - see front matter © 2008 Acta Materialia Inc. Published by Elsevier Ltd. All rights reserved.
doi:10.1016/j.actbio.2008.08.008

observe a Ti metal peak in the Ti 2p spectrum. In studies of the native oxide formed on Ti–6Al–4V, lower oxidation states of Ti were also observed [5,6]. The oxide thickness in many studies is found to vary between 2 and 8 nm, and considering that the analytical depth of XPS is of approximately 5 nm, the absence of intermediate oxidation states in the recorded data is probably a result of the intermediate oxides occurring at the interface beyond the probed analysis depth. In aqueous and simulated body fluid environments, it is generally accepted that the oxide film is predominantly TiO_2, but small amounts of intermediate oxides, Ti_2O_3 and TiO have also been reported [6–8].

Ti alloys with good mechanical and corrosion resistance properties, such as Ti–6Al–4V and Ti–6Al–7Nb, have been quite extensively used in biomedical applications [2]. Sittig et al. [3] have investigated the oxide film composition using XPS for commercially pure Ti (cp-Ti), Ti–6Al–4V and Ti–6Al–7Nb alloys surface treated by mechanical polishing, passivation in HNO_3 solution or acid etching in $HNO_3 + HF$ solution. The oxide film formed on polished cp-Ti was composed mainly of TiO_2, with small concentrations of TiO and Ti_2O_3 at the Ti/oxide interface. The oxide film grown on polished Ti–6Al–7Nb showed the formation of Al_2O_3 and Nb_2O_5 in addition to TiO_2 with the relative concentrations of Al and Nb in the oxide being similar to that of the bulk. For Ti–6Al–4V, the surface concentration of Al was increased and that of V decreased compared to the bulk. There is concern about the potential toxic nature of Al and V cations released into the body as a result of metal corrosion of these alloys. Consequently, a new alloy composition, Ti–13Nb–13Zr, was developed in the 1990s for biomedical applications. This alloy has good corrosion resistance, improved biocompatibility and an elastic modulus similar to that of bone [9–11]. Lopéz et al. [9] have investigated the oxide film naturally grown on a Ti–13Nb–13Zr alloy by XPS. Their results showed that Zr was strongly enriched and Nb depleted in the oxide layer. Yu and Scully [10] found that β-Ti–13Nb–13Zr exhibits improved corrosion resistance when compared to other implant alloys such as cp-Ti or Ti–6Al–4V in both a simulated physiological solution (Ringer's solution) and a simulated occluded cell environment (5 M HCl). Khan et al. [11] studied the corrosion behaviour of Ti–6Al–4V, Ti–6Al–7Nb and Ti–13Nb–13Zr in various protein solutions and found that the corrosion resistance of the three alloys is similar in these environments.

Despite their high corrosion resistance and biocompatibility, the surface properties of Ti alloys can be improved by treatments to yield surfaces with more suitable properties for biomedical applications. Calcium compounds, especially hydroxyapatite (HA), are known to promote osseointegration and surface treatments that favour the growth of these compounds on Ti and Ti alloys and are the subject of much current research on biomaterials [1,2,12–14]. Many workers studying osseointegration of Ti alloys agree that the formation of a rougher gel-like layer with a high surface area and increased concentration of Ti–OH surface species, on the outer surface of the passive film of Ti, is important in promoting the growth of apatite [1,2]. Such surface active groups can be formed by different methods; for instance, NaOH treatments have been employed [12,13]. Wang et al. [12] exposed Ti in a 5 M NaOH solution at 60 °C for 24 h and suggested that this treatment results in the formation of an outer sodium titanate gel layer. Subsequent immersion in simulated body fluid (SBF) (a solution containing inorganic ions in concentrations similar to that of human blood plasma) induced bone-like apatite formation. Takadama et al. [13] investigated the formation of apatite on a Ti–6Al–4V alloy using similar NaOH solution conditions, but followed by thermal treatment. Using X-ray diffraction and XPS methods, these authors suggested that the alkaline treatment induces sodium titanate formation, which upon immersion in the SBF solution leads to the formation of surface Ti–OH groups. These groups then induce the growth of calcium titanate and amorphous calcium phosphate.

Another method of promoting the formation of a hydroxide-rich surface is by sol–gel deposition. From dipping Ti substrates into a Ti sol–gel solution and then heating to 500 °C for 10 min, Li et al. [14] deposited a titania gel on Ti. Immersing this surface in SBF solution resulted in formation of a poorly crystallized apatite layer similar to that grown on bone (Ca deficient and with carbonate replacing phosphate and hydroxyl groups in the structure).

Hydrogen peroxide (H_2O_2) can also stimulate the growth of a hydrated Ti oxide surface layer. H_2O_2 is a well-known oxidizing agent, promoting the cathodic reaction:

$$H_2O_2 + 2H^+ + 2e^- \rightarrow 2H_2O \quad [E^\circ = 1.77 - 0.059pH\,(V)]$$

that results in an enhanced corrosion/oxidation rate [15,16]. Exposure to H_2O_2 causes thickening and roughening of the oxide on Ti [17–21].

Implantation of materials into the body causes an inflammatory response and the generation of H_2O_2 by inflammatory cells into the extracellular space is an accepted biochemical mechanism [15]. Tengvall et al. [15,16] proposed that the end-product of Ti implanted into the body is the formation of a duplex oxide with a mostly TiO_2 inner layer and a stable, hydrated TiOOH gel-like oxide outer layer with good ion and protein exchange properties. Proteins, proteoglycans, inorganic ions and other macromolecules will be incorporated into this gel-like outer layer and provide a surface to which fibroblast and osteoblast cells readily attach.

Pan et al. [17,18] studied such processes using surface analytical techniques and their work is of particular relevance to the current study. Pan et al. investigated the effects of exposing commercially pure Ti to a phosphate-buffered saline (PBS) solution, with and without the addition of 100 mM H_2O_2 [17], after exposure to a minimal essential medium (MEM) solution (a solution composed of salts, amino acids, vitamins and other

components essential to cellular growth), with and without the presence of osteoblast-like cells [18]. After immersion in the PBS solution for up to 30 days, they found that the presence of H_2O_2 facilitated thickening of the Ti surface oxide from thicknesses of 10 nm to 40 nm [17]. XPS results showed that exposure in the saline solution (with and without H_2O_2) resulted in no nitrogen peak being observed [18]. For samples that had been previously immersed in MEM, either with or without the H_2O_2 pretreatment, approximately 10 at.% N was found and the N concentration increased to approximately 15 at.% when cells were present, suggesting the adsorption or incorporation of proteins into the surface. Concerning inorganic ion take-up, for samples exposed to the PBS solution (in the absence of H_2O_2) and then immersed in the MEM (without cells), no P and Ca was observed by XPS. A substantial carbon component was observed at around 287 eV and assigned to carbonate (rather surprisingly as carbonates normally have binding energies around 289 eV). The authors suggest that a hydroxycarbonate apatite-like (HCA-like) layer is being formed at the surface. On the PBS solution + H_2O_2 surface exposed to the MEM solution, both P and Ca were observed at concentrations of 1–3 at.%, but the "carbonate" peak had a low intensity, hence the formation of an HA-type layer rather than an HCA-like layer is implied. However, the presence of cells in the MEM solution again leads to similar concentrations of P and Ca being found at the surface, but a high "carbonate" peak intensity is observed, suggesting the formation of an HCA-like layer at the surface. Using atomic absorption spectrophotometry, the authors also found that the calcium content of the cells attached to the surface increases steadily as a function of time, which is indicative of mineralization. They concluded that (i) mineralization of the surface seems to be related to phosphate, calcium and carbonate ion incorporation into the surface oxide and precipitation of an HCA-like compound and (ii) the HCA-like layer is promoted by the H_2O_2 pretreatment and the presence of osteoblast-like cells [18].

Inserting implants into living tissue causes inflammatory responses with the biological formation of H_2O_2 and other species in the vicinity of the implant [15,16]. Consequently, immersion of implants in biological solutions with the addition of H_2O_2 will mimic the environment found for an implant when it is first inserted into the body.

In this study, the electrochemical behaviour and surface chemistry of a Ti–13Nb–13Zr alloy immersed in MEM (both with and without the addition of H_2O_2) have been investigated using electrochemical impedance spectroscopy (EIS) and XPS. Scanning electron microscopy (SEM) and cytotoxicity results will also be presented. The work aims to examine the apatite-forming ability of this Ti alloy in biological media and provide information on the surface chemical processes taking place in the body at the implant–tissue interface.

2. Materials and methods

The near-β Ti–13Nb–13Zr alloy used in this investigation was prepared by Schneider [22] by arc melting (99.9%) pure Ti and Nb, together with Zr containing 4.5% Hf, under argon, using a non-consumable electrode. To homogenize the material, it was heat treated at 1000 °C for 1 h, water cooled, and subsequently cold forged to 6.5 mm in diameter. After cold forging, the alloy was heat treated. The chemical composition of the material was determined by inductively coupled plasma-atomic emission spectroscopy (ICP-AES) and is shown in Table 1.

2.1. Electrochemical tests

Electrodes for electrochemical tests were prepared by epoxy cold resin mounting of the Ti alloy samples. The sample surface was prepared by progressively grinding with silicon carbide paper up to #2000, followed by mechanical polishing with a 1 μm diamond paste. An area of 0.33 cm^2 of the working electrode was exposed to the electrolyte. The open-circuit potential (OCP) was measured as a function of time in MEM solution. The MEM solution composition is shown in Table 2. This solution was naturally

Table 2
Chemical composition of MEM solution

Inorganic salts	mg l^{-1}	Amino acids	mg l^{-1}
$CaCl_2$ (anyd.)	220.00	L-Arginine·HCl	126.00
KCl	400.00	L-Cystine·2HCl	31.00
$MgSO_4$ (anyd.)	98.00	L-Glutamine	292.00
NaCl	6800.00	L-Histidine·HCl·H_2O	42.00
$NaHCO_3$	2200.00	L-Isoleucine	52.00
$NaH_2PO_4·H_2O$	140.00	L-Leucine	52.00
		L-Lysine·HCl	73.00
Vitamins		L-Methionine	15.00
D-Ca pantothenate	1.00	L-Phenylalanine	32.00
Choline cloride	1.00	L-Threonine	48.00
Folic acid	1.00	L-Tryptophan	10.00
Inositol	2.00	L-Tyrosine (disodium salt)	52.00
Niacinamide	1.00	L-Valine	46.00
Pyridoxal·HCl	1.00	Other components	
Riboflavin	0.10	D-Glucose	1000.00
Tiamine·HCl	1.00	Red phenol	10.00

Table 1
Elemental composition of Ti–13Nb–13Zr alloy (wt.%)

Element	C	H	N	O	S	Hf	Fe	Nb	Zr	Ti
wt.%	0.035	0.011	0.04	0.078	<0.001	0.055	0.085	13.18	13.49	Bal.

Table 3
Chemical composition of PBS solution ($g\,l^{-1}$)

NaCl	Na_2HPO_4	KH_2PO_4
8.77	1.42	1.36

aerated and the pH was maintained at 7.6 with the addition of $NaHCO_3$. For one batch of samples, 100 mM of H_2O_2 was added to the MEM solution. The samples remained immersed in the MEM solution (with or without H_2O_2) for 72 h. At this point; some samples were removed for XPS analysis. XPS analysis was also carried out on samples which had the same 72 h open-circuit MEM exposure but were initially polarized at 4 V for 30 min to promote oxide film growth. Other samples were immersed in the MEM (with or without H_2O_2) for 125 days and then removed for SEM examination. EIS and potentiodynamic polarization tests were carried after 15 and 125 days of immersion. A PBS solution, the composition of which is given in Table 3, was used as the electrolyte in the EIS and polarization tests.

A three-electrode cell arrangement was used for the electrochemical measurements, with a saturated calomel reference electrode (SCE) as reference electrode and a platinum wire as the auxiliary electrode. All the potentials measured are referred to the SCE electrode. Potentiodynamic polarization scans were carried out at a scan rate of 0.1 mV s^{-1} in the range from −800 to 3000 mV using an EG&G273A potentiostat. The EIS tests were undertaken using a Solartron Model SI 1255 Frequency Response Analyzer coupled to a Princeton Applied Research (PAR) Model 273A Potentiostat/Galvanostat. The EIS measurements were obtained at the OCP in a frequency range between 10^5 and 10^{-2} Hz with an applied AC signal of 10 mV (rms), and at a data collection rate of six points per decade. The temperature was maintained at 37 °C by immersing the 200 ml electrochemical cells in a thermostatic bath. The polarization and EIS tests were carried out in triplicate to monitor the reproducibility of the results. Data fitting of the EIS experimental results to the equivalent circuit was performed using the Zview software.

2.2. XPS analysis

XPS was performed with a VG Scientific ESCALAB mk II employing a non-monochromated Al K_α source running at 340 W power and a spherical sector analyzer. Due to the low concentration of many elements, survey spectra of the bulk coating were then recorded at 100 eV pass energy and narrow scans at 50 eV pass energy (step width of 0.1 eV). The take-off angle was 45°. Curve fitting was performed using a mixed Gaussian–Lorentzian lineshape and the spectra were quantified using instrument-modified Wagner sensitivity factors after a Shirley background subtraction. The spectra were charge referenced by assigning the adventitious C 1s peak to 285.0 eV.

2.3. Cytotoxicity tests

The cytotoxicity assay of the biomaterial was carried out according to ISO 10993-5 [23]. The cell line recommended for the test is a preferred established cell line obtained from recognized repositories such as American Type Culture Collection (ATCC). Chinese hamster ovary cells (ATCC CHO K1) were used in this investigation.

2.4. Extract preparation

ISO 10993-5 states that the ratio between the surface area of the material and the volume of the extraction vehicle should be in the range of 0.5–6.0 $cm^2\,ml^{-1}$. Hence, 5 cm^2 samples of Ti–13Nb–13Zr were sterilized by autoclaving at 120 °C for 20 min, 5 ml of RPMI 1640 was added and the samples incubated at 37 °C for 48 h. The extract obtained was employed for the cytotoxicity assay.

2.5. Cytotoxicity assay

Chinese hamster ovary cells were grown in a culture medium composed of RPMI 1640 containing 10% fetal calf serum and 1% antibiotics, in a plastic tissue culture flask at 37 °C in a humidified 5% CO_2 air incubator. After confluent monolayer propagation, the culture medium was removed and the cells were washed with PBS. The culture was treated with 0.25% trypsin solution to detach the cells from the culture tissue flask. After trypsination, cells were transferred to a screw-capped plastic tube, centrifuged and washed with PBS. The cells were resuspended in culture medium and the concentration was adjusted to 60,000 cells ml^{-1}. Ninety-six well tissue culture microtiter plates were prepared by the addition of the biomaterial extract and serially diluted (100, 50, 25, 12.5 and 6.25%), 50 ml per well in quadruplicate, followed by the addition of 50 ml of the cell suspension (3000 cells). A blank was prepared of the culture medium without cells and a negative control was prepared of the culture medium instead of extract plus cells, both in quadruplicates. An extract solution of TiO_2 and 0.3% phenol solution were assayed as negative and positive material controls, respectively. The microplates were incubated in a 5% CO_2 humidified atmosphere. After 72 h, 20 µl of a mixture (20:1) of 0.2% MTS and 0.09% PMS in PBS were added to the test wells and left for 2 h. The dye incorporated was measured by reading the absorbance at 490 nm in a microplate reader against the blank.

3. Results

3.1. Electrochemical tests

The OCP variation of the Ti–13Nb–13Zr alloy as a function of immersion time in the MEM solution at 37 °C is shown in Fig. 1. The OCP value was approximately −650 mV immediately after immersion, but it rap-

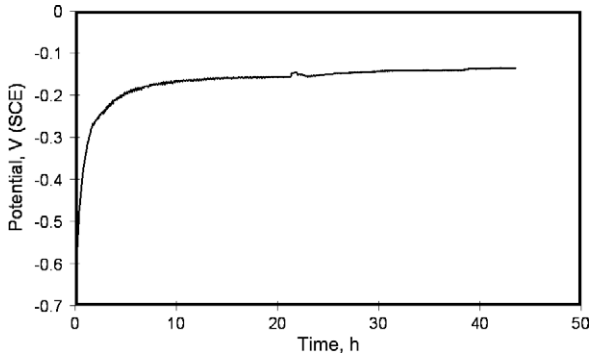

Fig. 1. Open-circuit potential variation as a function of immersion time for the Ti–13Nb–13Zr alloy immersed in MEM at 37 °C.

idly increased and after 10 h reached a stable value of approximately −160 mV. There is a slow increase in the potential as a function of time, and after 40 h, the OCP reached a value of around −135 mV. The increase in the potential is indicative of surface film growth on the Ti–13Nb–13Zr alloy, showing that it is faster during the first 10 h of immersion, but film growth continues as a function of time.

Figs. 2a and b show the polarization curves obtained in PBS for the Ti–13Nb–13Zr alloy after 15 and 125 days of immersion in the MEM solution, with or without H_2O_2, respectively, while Fig. 2c compares the polarization curves obtained in PBS for samples after 125 days of immersion in both solutions. All the polarization curves present approximately the same corrosion potential (−290 mV), and corrosion current densities obtained from these curves were very small (of the order of nA cm^{-2}), indicating passive behaviour for Ti–13Nb–13Zr in both solutions. However, their shapes are considerably different. It can be observed in Fig. 2c that the potential for the onset of oxide growth shifts in the positive direction with both increasing immersion time and presence of H_2O_2, providing evidence for thickening of the compact oxide film. According to Blackwood et al. the rate of dissolution and the stability of the oxide film formed on Ti depend on the rate at which the oxide film has been formed as well as on solution composition and temperature [24]. Lower corrosion current densities were associated with the samples that had been immersed for longer time periods, as shown in Fig. 2a and b, corroborating the results of OCP vs. time measurements, that indicates oxide film thickening. Fig. 2c shows that the samples exposed for 125 days in the MEM + H_2O_2 solution exhibit a higher resistance to oxide film dissolution as lower current densities up to 1300 mV are observed compared to those exposed in the MEM solution without H_2O_2. For some samples there is a large current density increase at potentials around 1300 mV. For these samples, the current density reaches a maximum at approximately 1700 mV that was followed by a current decrease to values of the order of μA cm^{-2} at potentials of 3000 mV. Observation of the polarized samples was carried out by SEM and no pits or any significant modification was found as a result

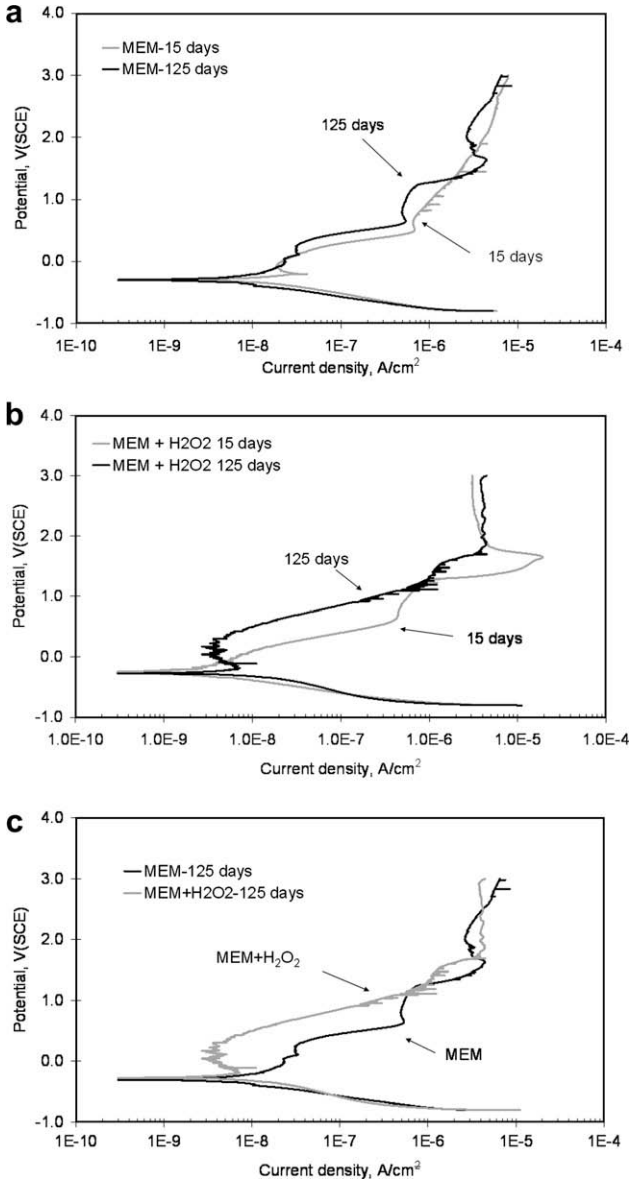

Fig. 2. Potentiodynamic polarization curves of Ti–13Nb–13Zr alloy after: (a) 15 or 125 days of immersion in MEM; (b) 15 or 125 days of immersion in MEM + H_2O_2; and (c) 125 days of immersion in MEM or MEM + H_2O_2. Scan rate: 0.1 mV s^{-1}.

of the polarization, showing that the current increase at approximately 1300 mV was not due to localised breakdown of the oxide film. Kolman and Scully [25,26] reported that pitting in chloride solutions is not found on Ti alloys up to very high anodic potentials. The current density increase might either be associated with the oxygen evolution reaction [25,26] or to changes in the valence state of one of the cationic species present in the oxide film.

Figs. 3 and 4 show experimental and fitted EIS obtained for the Ti–13Nb–13Zr alloy after 15 and 125 days in MEM and MEM + H_2O_2, respectively, while Fig. 5 compares the experimental EIS spectra obtained after 125 days of immersion in MEM and MEM + H_2O_2. Higher phase angles (around −80°) are seen at medium to high frequencies

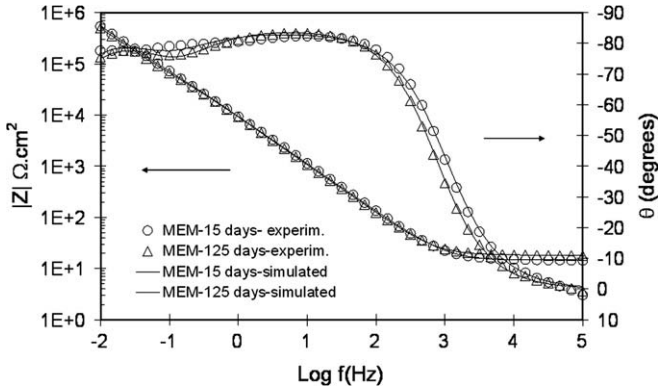

Fig. 3. Experimental and simulated EIS Bode diagrams for Ti–13Nb–13Zr alloy obtained after 15 or 125 days of immersion in MEM.

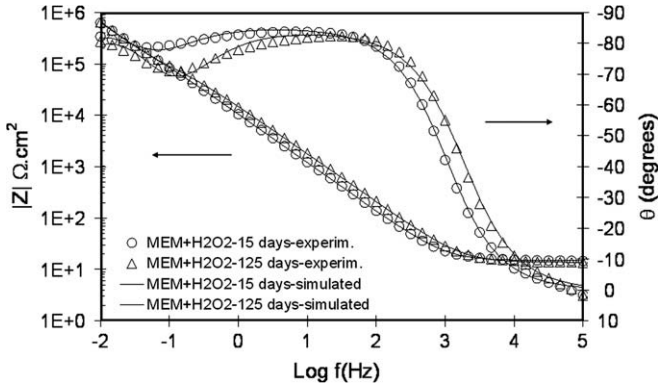

Fig. 4. Experimental and simulated EIS Bode diagrams for Ti–13Nb–13Zr alloy obtained after 15 or 125 days of immersion in MEM + 100 mM H_2O_2.

(0.1–1 kHz) in the EIS spectra of the samples which were immersed in MEM for longer periods, indicating the presence of a more capacitive and thicker film. These high phase angles are typical of passive materials. The emergence of two separate and distinct time constants increased with time of immersion. According to the literature [27,28], the two time constants are related to the formation of a duplex oxide film, composed of a barrier layer with a lower frequency time constant and a porous outer layer, with a higher frequency time constant. The high impedance values ($10^6\ \Omega\ cm^2$) at low frequencies are also indicative of passive behaviour for the Ti–13Nb–13Zr alloy in all solutions (MEM and MEM + H_2O_2). These results show that the oxide layer is providing good corrosion protection of the underlying metal.

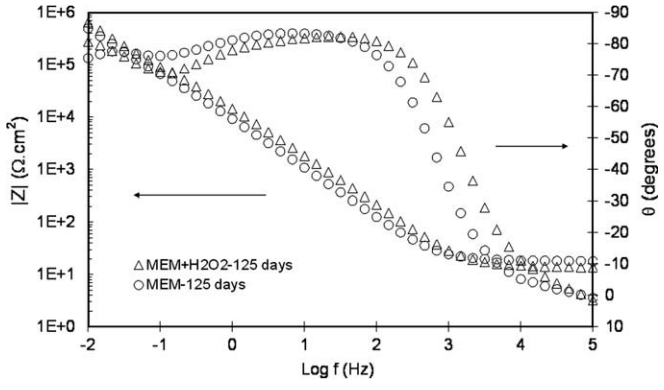

Fig. 5. Experimental and simulated EIS Bode diagrams for Ti–13Nb–13Zr alloy obtained after 125 days of immersion in MEM or MEM + 100 mM H_2O_2.

The equivalent electric circuit shown in Fig. 6 was used to simulate the experimental results. This circuit contains two constant-phase elements (CPE_p and CPE_b) in parallel with resistances R_p and R_b, respectively. This equivalent circuit was used by Scully and co-workers [25–27] to fit the experimental data recorded on Ti and Ti alloys in aqueous media and was used to fit the experimental data recorded in these experiments. It has been proposed that the oxide layer on Ti and Ti alloys has a duplex structure composed of an inner barrier layer and an external porous layer [28,29]. In the equivalent circuit, CPE_b and R_b represent the capacitive and resistive behaviour of the barrier layer, and CPE_p and R_p, the same for the porous layer. It is the barrier layer which affords the good corrosion resistance of Ti alloys [27]. The capacitance of the barrier layer, CPE_b, is responsible for the high phase angles at low frequencies, whereas the electronic and ionic resistance of the barrier layer, R_b, is responsible for the semiconductive properties of this layer. The porous layer is highly defective and contains microscopic pores where species from the electrolyte are incorporated. Pan et al. [17,18] have proposed that the porous layer promotes osteointegration by allowing the incorporation of inorganic ions from solution.

Equivalent circuit parameters obtained from fitting the EIS experimental data shown in Table 4. The values presented in this table show that even after 125 days of immersion in the MEM or MEM + H_2O_2 solution, the resistance of the barrier layer was of the order of $M\Omega\ cm^2$. These high values support the low current density values (of the order of nA cm^{-2}) obtained, showing passive behaviour for the Ti alloy.

In this work, it was assumed that the oxide layer might be represented by a parallel-plate capacitor and the equa-

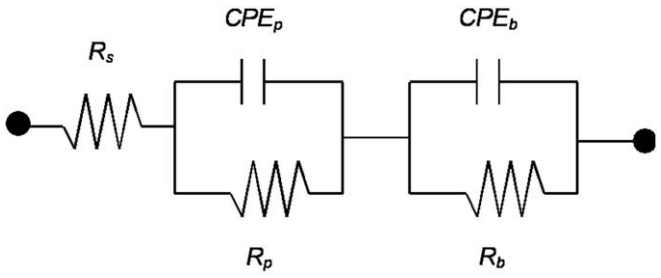

Fig. 6. Equivalent electric circuit used for fitting the experimental EIS data obtained for the Ti–13Nb–13Zr alloy in MEM or MEM + H_2O_2 solutions.

Table 4
Electrical parameters and error values obtained from fitting EIS experimental data to the equivalent circuit given in Fig. 6

Electrical element		Treatment condition							
		MEM				$MEM + H_2O_2$			
		15 days		125 days		15 days		125 days	
		Value	Error (%)	Value	Error (%)	Value	Error (%)	Value	Error (%)
R_s	$\Omega\,cm^2$	14.65	0.49	18.33	0.28	14.95	0.41	13.79	0.69
R_p	$k\Omega\,cm^2$	20.47	9.90	15.44	4.56	48.77	6.20	46.71	4.03
CPE_p	$\mu F\,s^{\alpha-1}\,cm^{-2}$	75.42	3.10	68.89	1.7	45.83	1.06	22.36	1.55
	α_p	0.88	0.44	0.93	0.30	0.88	#	0.89	0.27
CPE_b	$\mu F\,s^{\alpha-1}\,cm^{-2}$	26.70	0.99	26,60	0.52	25.26	0.92	24.22	1.08
	α_b	0.95	#	0.94	#	0.99	#	0.99	#
R_b	$M\Omega\,cm^2$	4.27	10.39	3.50	5.73	8.85	14.83	5.75	14.86
χ^2		0.0017		0.0006		0.0013		0.0025	

Value was fixed.

tion $C = \varepsilon\varepsilon_0 A/d$ where C is the capacitance ε is the dielectric constant of the porous layer, ε_0 is the dielectric permittivity of vacuum, A and d are the area and thickness of the oxide layer, respectively, applies. Although there is some controversy in the literature on the use of the EIS to accurately estimate the oxide film thickness for Ti-based materials at open-circuit potentials [30], some approximate relative values regarding oxide film thickness can be estimated from the capacitance values obtained [31]. Based on the capacitance values for the porous outer layer, the following changes to the thickness of this layer can be extracted from the results. The increase in the outer porous layer thickness from 15 to 125 days in the MEM solution was only about 10%, compared to about 100% in the MEM + H_2O_2 solution. Furthermore, compared to the samples exposed in MEM, the samples exposed in MEM + H_2O_2 showed an increase in thickness of 60% after immersion for 15 days and 200% after immersion for 125 days. These results show that H_2O_2 has a distinct effect in increasing the porous layer thickness over a prolonged time period.

3.2. XPS results

Table 5 lists the elemental compositions derived from XPS for the Ti–13Nb–13Zr alloy after different exposures: (a) as-received (reference); (b) exposed to MEM at the free corrosion potential for 72 h; (c) kept at a potential of 4 V for 30 min then exposed to MEM for 72 h; (d) exposed to MEM + 100 mM H_2O_2 at the free corrosion potential for 72 h; (e) kept at 4 V for 30 min then exposed in MEM + H_2O_2 for 72 h. The corresponding XPS C 1s, Ti 2p, O 1s and N 1s and spectra for these samples are shown in Fig. 7a–d. Zr and Nb 3d spectra from the as-received alloy and representative Ca 2p and P 2p spectra for the samples exposed to the 72 h in MEM solution are given in Fig. 8. (The results for the samples kept at 4 V for 30 min are presented in addition to those without this initial conditioning to highlight the consistency in the XPS results for these 72 h exposures.)

Some general comparisons between the spectra can be made, before looking at the various exposures in detail. The C 1s peak shape is comparable for all samples; there is no indication of a substantial carbonate peak being present. The Ti 2p spectra for the as-received and MEM (without H_2O_2) exposed samples are very similar, with TiO_2 at 458.6 eV being the predominant component. A small Ti metallic peak at 453.9 eV can be observed for the as-received sample, indicating that the total overlayer thickness on the alloy is thicker for the MEM-exposed samples. The O 1s peak for the as-received and MEM (without H_2O_2) exposed samples exhibit a large oxide component at 530.2 eV and secondary contributions from phosphate/hydroxide and adsorbed water at higher energies (discussed in detail later), whereas the MEM + H_2O_2 samples have a distinct primary component at 531.6 eV corresponding to phosphate/hydroxide. There is a noticeable shift in the N 1s peak between the as-received and MEM (without H_2O_2) samples compared to the MEM + H_2O_2 samples. The former exhibit a peak position of 400.2 eV, whereas the latter shift to a lower binding energy of 399.8 eV.

Considering first the as-received Ti–13Nb–13Zr alloy, the peak positions of the Ti 2p, Zr 3d and Nb 3d peaks

Table 5
XPS-determined surface elemental concentrations for the Ti–13Nb–13Zr alloy exposed to different conditions

Treatment condition	Ti	Zr	Nb	O	Ca	P	N	Na	C
Reference	7.6	0.7	0.6	30.4			2.1		58.6
MEM	9.0	1.0	0.9	40.0	2.4	1.8	3.9	1.2	39.8
MEM (4 V, 30 min)	6.9	0.6	0.5	29.3	1.3	2.0	4.7	1.0	53.8
MEM + H_2O_2	0.4	0.1	0.1	38.5	6.4	6.2	6.6	0.6	41.3
MEM + H_2O_2 (4 V, 30 min)	0.3	0.1	0.1	35.6	5.8	5.8	5.8	0.4	46.2

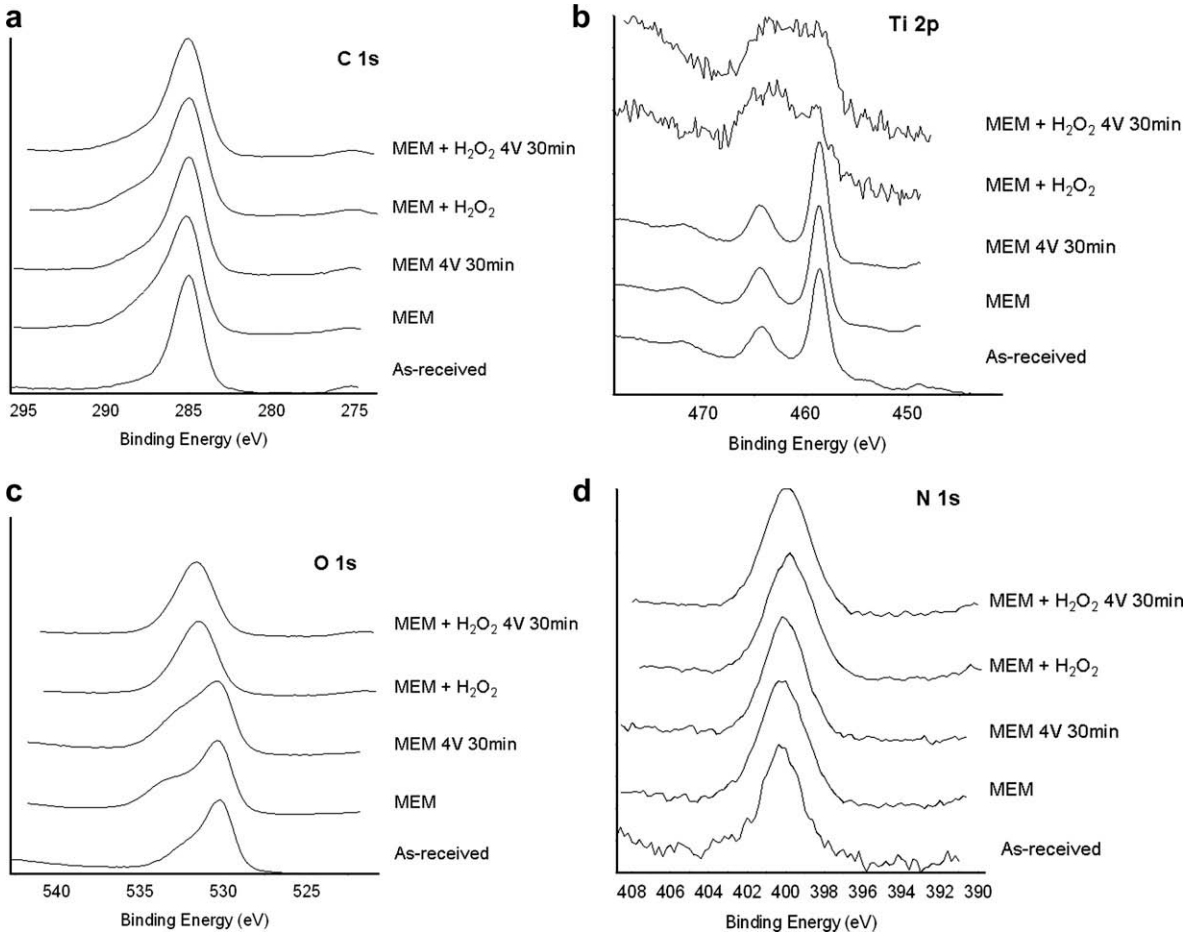

Fig. 7. XPS spectra for the Ti–13Nb–13Zr alloy after different exposures: (a) C 1s; (b) Ti 2p; (c) O 1s; (d) N 1s.

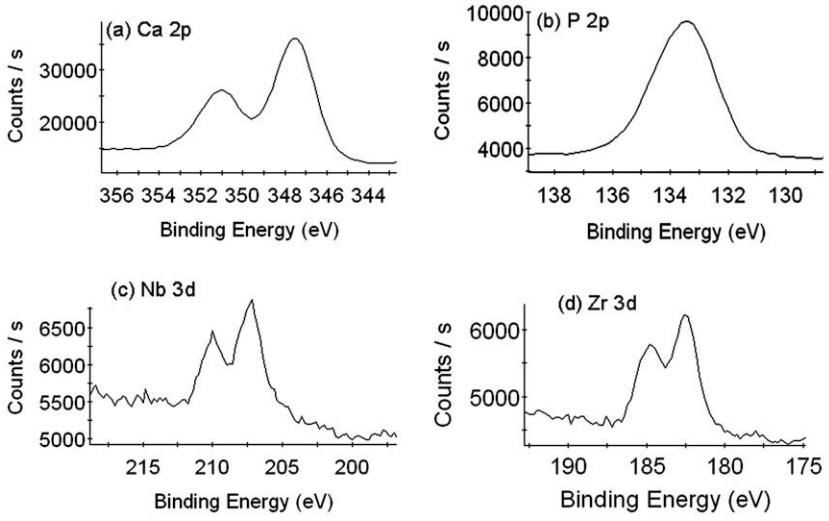

Fig. 8. XPS spectra for the Ti–13Nb–13Zr alloy: (a) Ca 2p peak for the sample immersed for 72 h in MEM + H_2O_2; (b) P 2p peak for the sample immersed for 72 h in MEM + H_2O_2; (c) Nb 3d peak for the as-received sample; (d) Zr 3d peak for the as-received sample.

are 485.6, 182.6 and 207.2 eV, respectively. All correspond to the expected binding energies for TiO_2, ZrO_2 and Nb_2O_5 [32]. A curve-fitted Ti 2p peak is shown in Fig. 9. In addition to the small Ti $2p_{3/2}$ metal peak at 453.9 eV and the predominant TiO_2 peak at 458.6 eV, fitting of the Ti $2p_{3/2}$ peak envelope required two small peaks at approximately

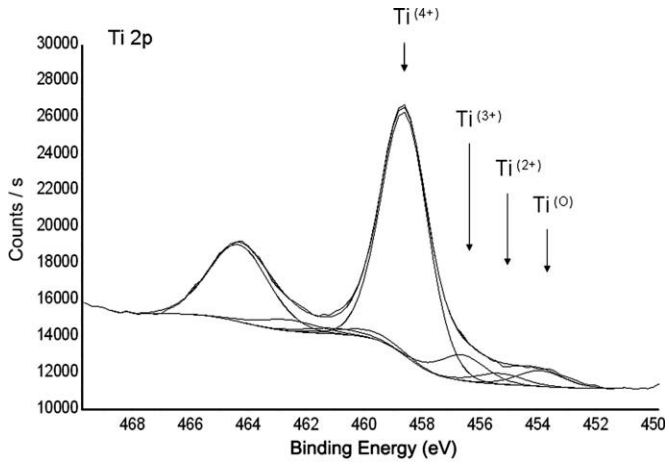

Fig. 9. Peak-fitted Ti 2p region for the as-received Ti–13Nb–13Zr alloy.

455.3 and 456.6 eV, indicating the presence of small concentrations of TiO and Ti_2O_3 at the metal/oxide interface. As all the metallic species are in their oxidized states, by neglecting the small metal peaks, the ratio of cationic species in the oxide compared to the bulk can be approximately determined from the relative atomic percentages of each element. Converting weight to atomic percentages for the metal concentrations given in Table 1, gives 84.1 at.% Ti, 7.8 at.% Nb and 8.1 at.% Zr. Consequently the bulk Ti/Nb and Ti/Zr at.% ratios are 10.8 and 10.4, respectively. From the values given in Table 5, the XPS-determined Ti/Nb and Ti/Zr cationic ratios in the oxide are 12.7 and 10.9. The cationic concentrations of Zr and Nb in the oxide are hence remarkably similar to the bulk concentrations of Nb and Zr and indicate that the only difference (if any) is a slight depletion of Nb in the oxide compared to the bulk. An O 1s peak fit for the as-received sample is shown in Fig. 10a. Three components are present corresponding to oxide at 530.2 eV, hydroxide at 531.7 eV and water at 533.0 eV, showing the presence of an outer hydroxide layer and adsorbed water at the surface of the oxide. The XPS peak position of N and low concentration at the surface are indicative of typical atmospheric contamination.

The specimens exposed to the MEM solution (without H_2O_2) show the formation of TiO_2, Nb_2O_5 and ZrO_2 to constitute the oxide layer on the Ti–13Nb–13Zr alloy. The Ti/Nb and Ti/Zr cationic ratios are 10.0 and 9.0, respectively, so again there is a negligible difference between the cationic concentrations in the oxide and the bulk metal concentrations. The O 1s peakshape (Fig. 10b) indicates that the surface formed in MEM solution is more hydrated than that on the air-formed oxide, with an increase in both the OH^- and H_2O component intensities. (However, the presence of P and Ca at the surface indicates the formation of a calcium phosphate compound and the overlap of PO_4^{2-} and OH^- components leads to an enhancement of the OH^- peak intensity.) There is a small Na Auger KL_1L_{23} peak at high binding energies. Ca and P are present at approximately 2 at.% and the P 2p

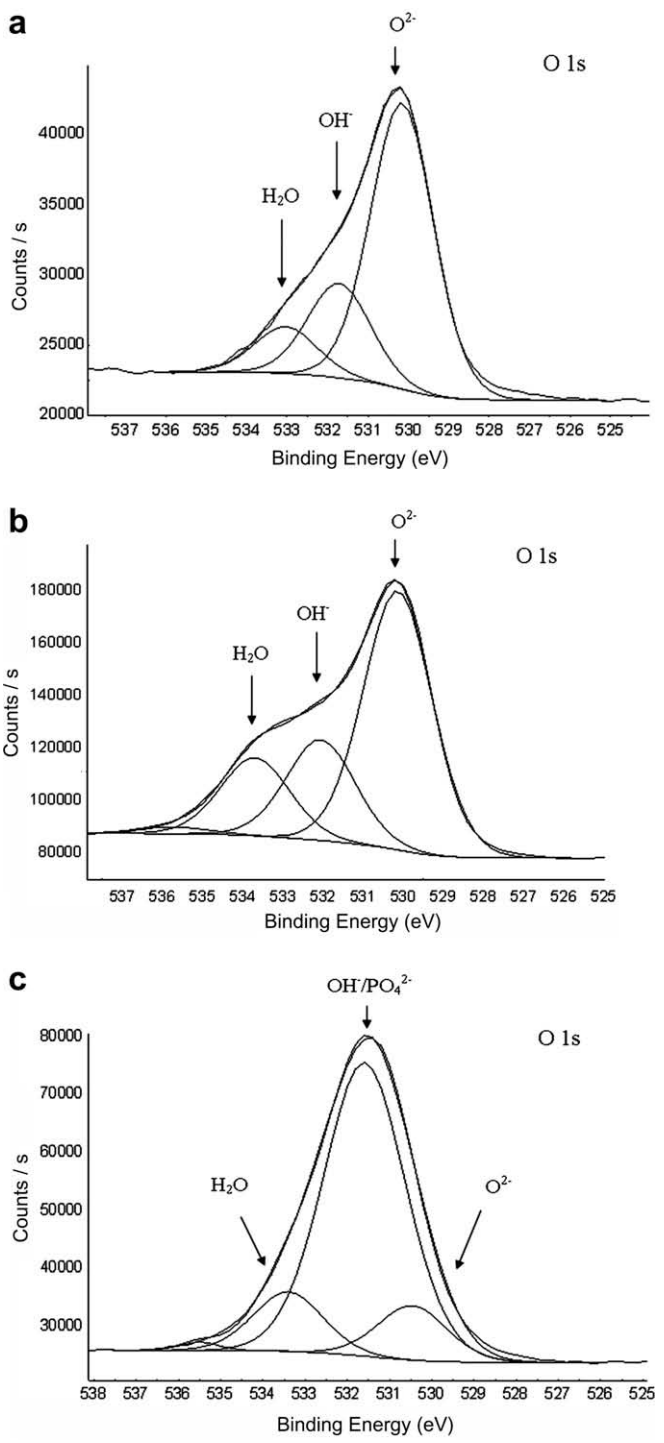

Fig. 10. Peak-fitted O 1s region for the Ti–13Nb–13Zr alloy: (a) as-received; (b) immersed in MEM solution for 72 h; (c) immersed in MEM + H_2O_2 solution for 72 h.

and Ca 2p peaks occur at 133.4 and 347.6 eV, respectively, corresponding to the peak positions expected for a number of calcium phosphate compounds [33]. The Ca/P ratio varied considerably between the two MEM exposures (without H_2O_2) and hence it is difficult to make a reliable assessment, but taking the averaged values for the two samples, the Ca/P ratio is approximately 1.0.

XPS has some difficulty in distinguishing between the different calcium phosphate minerals [33–35]. HA has a theoretical Ca/P ratio of 1.67 and there are a number of other calcium phosphate compounds with lower Ca/P ratios, including brushite ($CaHPO_4 \cdot H_2O$), which has a Ca/P ratio of 1.0. However, Kumar et al. have shown that brushite is soluble in aqueous solutions and (the more stable) HA is subsequently precipitated onto the surface [36]. Air-exposed bulk HA samples show an XPS-determined Ca/P ratio close to or slightly lower than the stoichiometric value of 1.67 [34,35,37], whereas a significant reduction in the Ca/P ratio (values close to 1.0) has been found in this and other XPS studies of HA formation in aqueous and physiological solutions [38–40]. Amrah-Bouali et al. [40] have studied the Ca/P ratio determined by XPS for HA exposed to a range of aqueous and physiological solutions and found that in all cases that the Ca/P ratio after exposure approaches 1.0. They concluded that the change in composition at the surface is related to reactions occurring in aqueous media and this reduction in the Ca/P ratio is most probably associated with the biological behaviour of HA. Furthermore, other workers using XRD to study the initial deposition of inorganic compounds onto hydrated titanium oxide surfaces in body fluid environments have clearly shown that apatite is the calcium phosphate compound deposited [13,14]. Hence, in spite of the possible ambiguity arising from the XPS results, it is reasonable to conclude that HA is the calcium phosphate compound being deposited in the MEM (and MEM + H_2O_2) in this work.

While performing the XPS, some differential charging was observed, suggesting incomplete formation of a HA surface layer (e.g. an island-like distribution). Immersion in the MEM solution also gives rise to the nitrogen concentration increasing to around 4 at.% from 2 at.% prior to insertion in the medium.

The addition of H_2O_2 to the MEM solution has a dramatic effect on the surface chemistry. Compared to the pure MEM solution, the Ti concentration is strongly reduced from about 8 to 0.4 at.%, with a concomitant increase in the Ca and P concentrations from approximately 2 to 6 at.%. At such low concentrations, the Ti 2p peak exhibits poor signal/noise ratios, but there is clearly a peak occurring at the same binding energy of TiO_2. Although the total Ti 2p peak envelope appears to extend over a similar binding energy range to the MEM-exposed sample, surprisingly there is no drop in the intensity between the Ti $2p_{3/2}$ and Ti $2p_{1/2}$ peaks. This may indicate the presence of a small concentration of Ti in a chemical state with a binding energy higher than that of TiO_2. The O 1s peak (Fig. 10c) shows the presence of a principal component at 531.6 eV, corresponding to PO_4^{2-}/OH^- groups of HA and two smaller peaks at 530.4 and 533.4 eV associated with O^{2-} and H_2O, respectively, consistent with other XPS O 1s spectra from HA layers [41]. Ca and P are both present at 6 at.% and a thick layer of HA was clearly formed during this exposure. As found for the pure MEM solution, the Ca/P ratio is again 1.0. Exposure to the MEM + H_2O_2 media also leads to an increase in the nitrogen concentration at the surface to approximately 6 at.% and to a reduction in the N 1s binding energy to 399.8 eV.

SEM images of the Ti–13Nb–13Zr alloy surfaces after 125 days of exposure in the MEM and MEM + H_2O_2 solutions are given in Fig. 11. In the MEM solution, the large number of discrete particles on the surface is representative of the island-like deposition of HA. For the sample exposed in the MEM + H_2O_2, the polishing marks on the metal are no longer visible and a generally smoother morphology is observed, indicative of thicker layer formation.

3.3. Cytotoxicity test

Cytotoxicity ($CT_{50\%}$) was estimated by plotting the mean percentage of surviving cells against the concentration of the extract (%) and determining the biomaterial extract concentration resulting in 50% inhibition of MTS uptake. Fig. 12 shows the results of the cytoxicity test. Comparing Ti–13Nb–13Zr with the negative control (TiO_2), the material could be considered non-cytotoxic. However, the phenol solution (positive control) showed a cytotoxic behaviour with an $IC_{50\%}$ value corresponding to an extract concentration of 15. Consequently, a 15% initial solution of phenol eliminates 50% of the cell population. The extracts prepared with Ti–13Nb–13Zr showed an $IC_{50\%}$ of approximately 100, and hence this alloy is non-toxic.

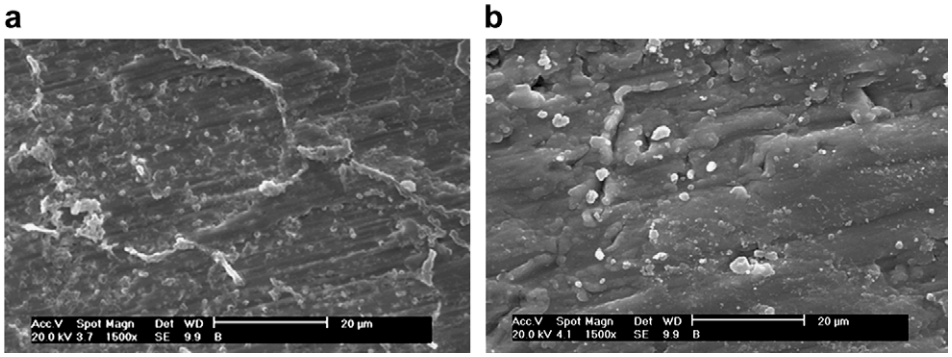

Fig. 11. SEM micrographs of Ti–13Nb–13Zr alloy after 125 days immersion in MEM: (a) without H_2O_2; (b) with 100 mM H_2O_2.

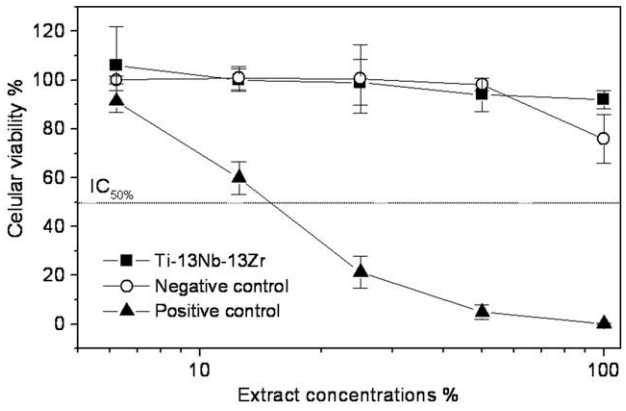

Fig. 12. Colony suppression curve of the cytotoxicity test for Ti–13Nb–13Zr alloy.

4. Discussion

The native oxide formed on the near-β Ti–13Nb–13Zr alloy is composed mainly of TiO_2, but also Nb_2O_5 and ZrO_2. The cationic ratios in the oxide are very similar to the bulk, indicating little or no preferential oxide formation. This is in contrast to the results of Lopez et al. [9], which show a strong enrichment of Zr and depletion of Nb in the oxide. It is considered here that the main role of Nb is to act as a β-stabilizer and that it has little effect on the surface properties of the alloy. Immersion in the MEM solution results in spontaneous passivation of the Ti–13Nb–13Zr alloy surface, and passivity is observed over a large potential range. The EIS results indicate that the passive film is composed of an inner barrier layer and an outer porous layer. The XPS results show the formation of small amount of HA at the surface, when exposed to the MEM solution. The HA has an island-like distribution on the surface. From the XPS, EIS and SEM results, it is apparent that the addition of H_2O_2 to the MEM solution results in the formation of a much thicker, but still porous, HA layer. H_2O_2 induces the formation of a hydrated oxide layer and drives a thickening and roughening of this layer. This thicker hydrated oxide layer provides an environment which strongly promotes the deposition of HA at the surface.

The XPS results presented in this investigation show some agreement and some disagreement with those reported by Pan et al. [18] for exposed Ti samples in MEM (with and without H_2O_2) for a period of 30 days. Pan et al. did not observe the deposition of Ca or P when exposed in the MEM solution, in contrast to the results observed here. In the MEM + H_2O_2 solution, Ca and P were found by Pan et al., but at lower concentrations to that seen here. Pan et al. report the formation of an HCA-like compound on the basis of a C 1s component at 287 eV being present in the spectra. This interpretation is highly questionable, since carbonate groups are normally observed at binding energies of around 289 eV [32]. Instead, it appears most likely that Pan et al. observed the formation of an HA compound as a result of exposure to MEM + H_2O_2, as found in this investigation.

The shape of the Ti 2p peak envelope for the samples is suggestive of there being higher binding energy peaks for Ti, above TiO_2. Although the authors have been unable to find any data for Ti compounds in the literature, in this HA environment, a high binding energy 2p peak might be expected if the Ti^{4+} cation is bonded to groups such as PO_4^{3-} of HPO_4^{2-} [42] or as TiOOH [43], rather than O^{2-} ions. Consequently, the Ti may become incorporated into the HA-type layer, substituting for Ca cations within the

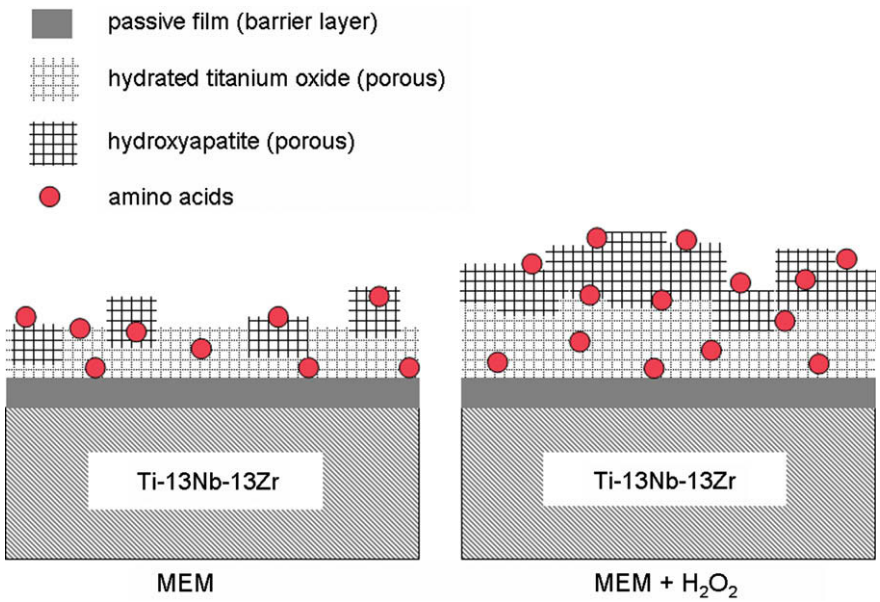

Fig. 13. Schematic diagram of the proposed surface structure which develops on the Ti–13Nb–13Zr alloy after 72 h immersion in MEM and MEM + H_2O_2.

structure [39,40] and or a TiOOH layer may form at the outer surface of the Ti alloy oxide [16]. Further work is required to resolve the exact chemical state and location of Ti cations within this surface region.

XPS N 1s intensities are often used as indicators of amino acid and protein adsorption in studies of biomolecular adsorption onto surfaces. Amino acids are known to act as corrosion inhibitors through chemisorption of these molecules to the metal surface [44,45] and adsorb onto surfaces in a matter of seconds. Formation of HA clearly takes many hours, and hence the observed increase in N concentration in the MEM and MEM + H_2O_2 exposures and the shift of the N peak position to lower binding energy values (corresponding to C–N or amine bonding) is indicative of a layer growing on the surface which is comprised of both HA and amino acids. This is in general agreement with the work of do Serro et al. [46] for Ti and HA-coated Ti samples exposed in Hanks' solution with the addition of bovine serum albumin in which the authors concluded that albumin initially adsorbs to the surface, followed by the slower deposition of and Ca and P ions. The results presented here show that as HA grows to form a thicker continuous and porous layer, amino acids continue to be incorporated in that layer.

This study has shown that in MEM solution, the near-β Ti–13Nb–13Zr is a corrosion-resistant, biocompatible metal and exhibits promise as a new medical alloy. Immersion of the Ti–13Nb–13Zr alloy in MEM solution results in the formation of an island-like distribution of HA and amino acids. The addition of H_2O_2 to the MEM solution strongly promotes the formation of a continuous nanocomposite layer of HA and amino acids. The reactions at the Ti oxide surface that are stimulated by the presence of H_2O_2 are complex [15,16], but the end result is the growth of a thicker, continuous but porous nanocomposite layer with an overall composition similar to that formed in pure MEM solution. A schematic diagram of the proposed surface structures which develop after 72 h immersion in MEM and MEM + H_2O_2 are shown in Fig. 13. Hence, for Ti alloys, release of H_2O_2 in the anti-inflammatory response is an important beneficial process as it serves to accelerate osseointegration. For Ti alloy implant surfaces in the body, in addition to amino acids, the extracellular material contains important proteins, such a proteoglycans [15,16]. It is to be expected that such proteins in addition to amino acids will become incorporated into the growing HA layer, forming a surface which favours osteoblast growth.

5. Conclusions

(1) The near-β Ti–13Nb–13Zr alloy is non-toxic and shows good corrosion resistance. The native oxide formed is mainly composed of TiO_2, but also Nb_2O_5 and ZrO_2. The cationic ratios in the oxide are very similar to those in the bulk, hence there is that no preferential oxidation taking place for this alloy.

(2) When immersed in MEM solution, the passive film of the Ti–13Nb–13Zr alloy is composed of an inner barrier layer and an outer porous layer. The addition of H_2O_2 has the effect of increasing the porous layer thickness over a prolonged time period (200% thickness increase after 125 days) and a concomitant strong reduction in the corrosion current density.

(3) Exposure for 72 h in the MEM solution results in the formation of a surface layer with an island-like distribution of HA and amino acids. The addition of H_2O_2 to the MEM solution strongly promotes the formation of a thicker, continuous but porous nanocomposite layer comprised of HA and amino acids.

(4) For Ti alloys, the release of H_2O_2 in the anti-inflammatory response is an important beneficial process as it accelerates the formation of the nanocomposite HA and amino acid (protein) layer, promoting osseointegration.

Acknowledgements

The authors are grateful to CNPq-Brazil for their financial support of this research. Dr. Baker thanks Mr. Lionel Pierquet and Miss Rosanna Grilli for their assistance with the XPS analysis and data treatment.

References

[1] Jones FH. Surf Sci Rep 2001;42:75.
[2] Liu X, Chu PK, Ding C. Mater Sci Eng R 2004;47:49.
[3] Sittig C, Textor M, Spencer ND, Wieland M, Vallotton P-H. J Mater Sci Mater Med 1999;10:35.
[4] McCafferty E, Wightman JP. Appl Surf Sci 1999;143:92.
[5] Ask M, Lausmaa J, Kasemo B. Appl Surf Sci 1989;35:283.
[6] Milošev I, Metikoš-Hukovic M, Strehblow H-H. Biomaterials 2000;21:2103.
[7] Huang YZ, Blackwood DJ. Electrochim Acta 2005;51:1099.
[8] Schutz RW. In: Baboian R, editor. Corrosion tests and standards: applications. Philadelphia (PA): ASTM International; 1995. p. 493–506.
[9] López MF, Gutiérrez A, Jiménez JA. Surf Sci 2001;482–485:300.
[10] Yu SY, Scully JR. Corrosion 1997;12:965.
[11] Khan MA, Williams RL, Williams DF. Biomaterials 1999;20:631.
[12] Wang CX, Wang M, Zhou X. Biomaterials 2003;24:3069.
[13] Takadama H, Kim H-M, Kokubo T, Nakamura T. Sci Technol Adv Mater 2001;2:389.
[14] Li P, Kangasniemi I, de Groot K, Kokubo T. J Am Ceram Soc 1994;77:1307.
[15] Tengvall P, Lundström I, Sjöqvist L, Elwing H, Bjursten LM. Biomaterials 1989;10:166.
[16] Tengvall P, Lundström I. Clin Mater 1992;9:115.
[17] Pan J, Thierry D, Leygraf C. J Biomed Mater Res 1996;30:393.
[18] Pan J, Liao H, Leygraf C, Thierry D, Li J. J Biomed Mater Res 1998;40:244.
[19] Wälivaara B, Aronsson B, Rodahl M, Lausmaa J, Tengvall P. Biomaterials 1994;15:827.
[20] MacDonald DE, Rapuano BE, Deo N, Stranick M, Somasundaran P, Boskey AL. Biomaterials 2004;25:3135.
[21] Wälivaara B, Lundström I, Tengvall P. Clin Mater 1993;12:141.
[22] S.G. Schneider, Ph.D. Thesis, Instituto de Pesquisas Energéticas e Nucleares, Sao Paulo, Brazil; 2001.

[23] ISO 10993-5; 1999. Available from: http://www.iso.org/.
[24] Blackwood DJ, Peter LM, Williams DE. Electrochim Acta 1988;33:1143.
[25] Kolman DG, Scully JR. J Electrochem Soc 1993;140:2771.
[26] Kolman DG, Scully JR. J Electrochem Soc 1994;141:2633.
[27] Yu SY, Brodrick CW, Ryan MP, Scully JR. J Electrochem Soc 1999;146:4429.
[28] Lavos-Valereto IC, Ramires I, Guastaldi AC, Costa I, Wolynec I. J Mater Sci Mater Med 2004;15:55.
[29] Pan J, Thierry D, Leygraf C. Electrochim Acta 1996;41:1143.
[30] Blackwood DJ. Electrochim Acta 2000;46:563.
[31] Assis SL, Costa I. Mater Corrosion 2007;58:329.
[32] NIST X-ray Photoelectron Spectroscopy Database, version 3.4. Available from: http://srdata.nist.gov/xps/.
[33] Landis WJ, Martin JR, Vacuum J. Sci Technol A 1984;2:1108.
[34] Chusuei CC, Goodman DW, Van Stipdonk MJ, Justes DR, Schweikert EA. Anal Chem 1999;71:149.
[35] Lu H, Campbell CT, Graham DJ, Ratner BD. Anal Chem 2000;72:2886.
[36] Kumar M, Dasarathy H, Riley C. J Biomed Mater Res 1999;45: 302.
[37] Massaro C, Baker MA, Consentino F, Ramires PA, Klose S, Milella E. J Biomed Mater Res 2001;58:651.
[38] Ribeiro CC, Gibson I, Barbosa MA. Biomaterials 2006;27:1749.
[39] Leadley SR, Davies MC, Ribeiro CC, Barbosa MA, Paul AJ, Watts JF. Biomaterials 1997;18:311.
[40] Amrah-Bouali S, Rey C, Lebugle A, Bernache D. Biomaterials 1994;15:269.
[41] Kačiulis S, Mattogno G, Pandolfi L, Cavalli M, Gnappi G, Montenero A. Appl Surf Sci 1999;151:1.
[42] Demri B, Muster D. J Mater Process Technol 1995;55:311.
[43] Welsh ID, Sherwood PMA. Phys Rev B 1989;40:6386.
[44] Olivares O, Likhanova NV, Gómez B, Navarrete J, Llanos-Serrano ME, Arce E, et al. Appl Surf Sci 2006;252:2894.
[45] Morad MMS, Hermas AE-HA, Aal MSA. J Chem Technol Biotechnol 2002;77:486.
[46] do Serro APVA, Fernandes AC, de Jesus B, Saramango V. Colloids Surf B Biointerfaces 1997;10:95.